

High pressure and temperature thermoelasticity of hcp osmium from ab initio quasi-harmonic theory

Xuejun Gong

*School of Physical Science and Technology, Xinjiang University, Urumqi, Xinjiang 830046, China and
International School for Advanced Studies (SISSA), Via Bonomea 265, 34136, Trieste, Italy*

Andrea Dal Corso

*International School for Advanced Studies (SISSA), Via Bonomea 265, 34136, Trieste, Italy and
IOM - CNR, Via Bonomea 265, 34136, Trieste, Italy*

(Dated: July 22, 2025)

We present a systematic ab initio study of the thermoelastic properties of hcp osmium as functions of temperature and pressure within the quasi-harmonic approximation (QHA). The precision of the Zero Static Internal Stress Approximation (ZSISA) and of the volume-constrained ZSISA (V-ZSISA) are rigorously assessed. For osmium, we find negligible deviations between ZSISA and a full free energy minimization (FFEM) approach. Also, the V-ZSISA approximation influences the results very little, as we found already in beryllium, despite the markedly different behavior of the c/a ratio with temperature in the two metals. Our QHA-derived ECs show excellent agreement with available experimental data in the temperature range of 5–301 K, outperforming the results obtained from the quasi-static approximation (QSA). Additionally, we report the pressure-dependent QHA ECs at 5 K, 301 K, and 1000 K, spanning pressures from 0 to 150 kbar.

I. INTRODUCTION

Osmium, an hexagonal close-packed (hcp) 5d transition metal, is notable for its exceptional physical properties, including the highest density among all elements, a remarkably high melting point (3306 K), and a bulk modulus comparable to that of diamond. Osmium is also often alloyed with platinum and iridium to enhance their mechanical performance. Its thermodynamic properties have been extensively investigated both experimentally [1] and theoretically [2–4]. Numerous theoretical studies have focused on its equation of state, structural parameters, and electronic properties under pressure, [5–7] but its elastic properties remain only partially characterized.

The temperature dependence of osmium’s elastic constants (ECs) has been experimentally measured at ambient pressure over the range of 5–301 K [8], and recent work has inferred the pressure dependence of C_{44} (from 0 to 2022 kbar) at room temperature from Raman spectroscopy data [9]. Theoretical calculations of osmium’s ECs at ambient pressure and 0 K have been conducted by several groups using ab initio methods within both the local density approximation (LDA) [10] and the Perdew-Burke-Ernzerhof (PBE) generalized gradient approximation. [11–15] However, some discrepancies still remain among the reported values. Additionally, the pressure dependence of osmium’s ECs has been computed at 0 K [16], but no theoretical data are available for the temperature-dependent elastic constants (TDECs) within either the quasi-static (QSA) or quasi-harmonic (QHA) approximations. Furthermore, the high-pressure and high-temperature regime remains entirely unexplored, with no measurements or calculations reported to date.

In a recent study, we introduced a computational work-

flow for calculating the TDECs of hcp metals and applied it to beryllium. [17] This methodology enables the calculation of both QSA and QHA ECs within the zero static internal stress approximation (ZSISA), where ionic positions are relaxed by minimizing the total energy at each strain. Additionally, the method allows for the quantification of the ZSISA approximation’s accuracy by comparing it to results obtained from full free energy minimization (FFEM). Furthermore, the effect of the volume-constrained ZSISA (V-ZSISA) can be assessed by comparing ECs computed along the 0 kbar isobar with those calculated along the stress-pressure curve (defined as the path in crystal parameters space where the stress is a uniform pressure) at 0 K. Although the QHA is computationally more demanding than the QSA, it has been demonstrated to provide superior accuracy for several face-centered cubic (fcc) and body-centered cubic (bcc) metals, making it essential for quantitative predictions. [17–21]

In this work, we apply this workflow to osmium, presenting a comprehensive analysis of its elastic properties. We compare the ZSISA QHA results with those obtained from FFEM at a selected geometry, and quantify the effects of the V-ZSISA approximation within QSA. QHA TDECs are calculated only within V-ZSISA. We further validate our approach by comparing the QSA and QHA TDECs with experimental data in the temperature range of 5–301 K and provide predictions for elevated temperatures up to 1600 K. Additionally, we report the pressure dependence of the ECs from 0 to 150 kbar at temperatures of 5 K, 301 K, and 1000 K, offering the first theoretical estimates of osmium’s elastic properties in this high-pressure, high-temperature regime. We anticipate that these predictions will serve as a valuable reference for future experimental investigations.

TABLE I. Equilibrium lattice constant (a), bulk modulus (B_T), and first and second pressure derivative of the bulk modulus (B'_T , B''_T) for osmium obtained from a fourth-order Birch-Murnaghan fit of the energy. Comparison of current calculations with previous studies and experimental data. At 295 K we report the adiabatic QHA bulk modulus B_S , while at 0 K $B_S = B_T$. The 1500 K QHA crystal parameters are also reported (see text).

		T (K)	a (a.u.)	c/a	B_T (kbar)	B'_T	B''_T (kbar ⁻¹)
This study	LDA	0	5.133	1.579	4489	4.7	-0.0015
This study	PBEsol	0	5.159	1.579	4328	4.7	-0.0016
This study	PBE	0	5.204	1.578	3984	4.8	-0.0018
		295	5.212	1.579	3914	4.9	
		1500	5.242	1.585			
Calc. [2]	LDA	0	5.132	1.574	4470	4.63	
Calc. [22]	PBE	0	5.20	1.577	4080	3.6	
Calc. [16]	PBE	0	5.187	1.577	3960		
Expt. [23]		300	5.1680	1.5794	3950	4.5	

TABLE II. Elastic constants compared with experiment and previous calculations. We report also the bulk modulus (B), the Young's modulus (E), the shear modulus (G), and Poisson's ratio (ν) of polycrystalline osmium derived from the elastic constants. PBE elastic constants including zero-point motion (ZPM) and adiabatic QHA elastic constants at 300 K are also reported. Frozen-ion elastic constants are obtained by applying a uniform strain to atomic positions, omitting further atomic relaxation.

	T (K)	a (a.u.)	$\frac{c}{a}$	C_{11} (kbar)	C_{12} (kbar)	C_{13} (kbar)	C_{33} (kbar)	C_{44} (kbar)	B (kbar)	E (kbar)	G (kbar)	ν
This study (LDA)	0	5.133	1.579	8191	2529	2487	9161	2851	4501	7173	2906	0.234
Ref. [13] (LDA)	0			8087	2647	2437	8886	2712	4454	6931	2793	0.241
Ref. [14] (LDA)	0			7890	3080	2390	9580	2890	4559	6928	2778	0.247
Ref. [15] (LDA)	0			8390	2460	2570	9250	2790	4576	7251	2934	0.236
Ref. [12] (LDA)	0	5.202	1.578	8945	2492	2456	10164	1622	4755	6402	2511	0.275
This study (PBEsol)	0	5.156	1.579	7948	2413	2366	8907	2788	4339	6999	2842	0.231
This study (PBE)	0			7332	2202	2170	8224	2585	3992	6476	2633	0.230
PBE (Frozen-ions)	0			7366	2168	2171	8224	2589	3993	6507	2649	0.228
This study (PBE)	0+ZPM	5.207	1.578	7262	2188	2162	8135	2555	3960	6405	2603	0.230
This study (PBE)	301	5.212	1.578	7104	2194	2174	7948	2465	3911	6213	2515	0.235
Ref. [13] (PBE)	0			7301	2469	2305	7983	2469	4081	6231	2501	0.246
Ref. [14] (PBE)	0			7150	2740	2020	8700	2650	4058	6340	2557	0.240
Ref. [16] (PBE)	0			7480	2090	2070	8220	2610	3957	6618	2710	0.221
Expt. [8]	0			7633	2279	2180	8432	2693	4105	6737	2747	0.226

II. THEORY: THERMODYNAMICS AND ELASTIC CONSTANTS

All thermodynamic calculations employ our in-house software package `thermo_pw` [24], which implements the quasi-harmonic approximation (QHA) as detailed in previous works [3, 18, 19, 25–28]. The workflow for calculating TDECs in hcp systems was established in Ref. [17]. For completeness, we outline the key theoretical framework below.

Within the QHA formalism, the Helmholtz free energy of a hexagonal crystal depends on temperature T and

lattice parameters $\xi = (a, c/a)$, decomposing into three contributions:

$$F(\xi, T) = U(\xi) + F_{ph}(\xi, T) + F_{el}(\xi, T), \quad (1)$$

where $U(\xi)$ represents the static DFT energy, $F_{ph}(\xi, T)$ the phonon vibrational free energy, and $F_{el}(\xi, T)$ the electronic excitation term. The vibrational component de-

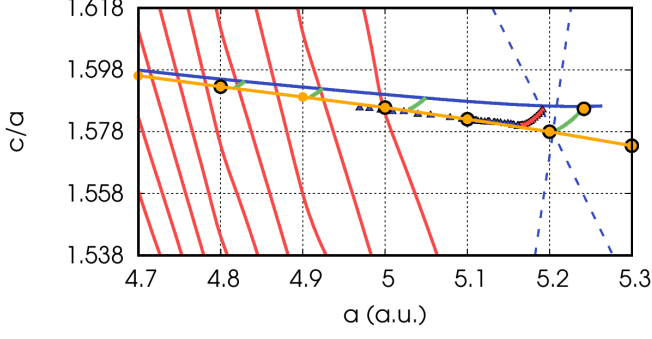


FIG. 1. Energy contours in the a and c/a crystal parameter plane (red lines). The intersection of the dashed blue lines pinpoints the energy minimum. The yellow and blue curves depict the curve where the stress is a uniform pressure at 0 K and 1500 K, respectively. The yellow dots mark the seven distinct geometries used to map the stress-pressure curve at 0 K. Black circles identify the geometries where TDECs were computed using the QHA. Green lines illustrate isobars at 0, 500, 1000, and 1500 kbar. The specific geometry at 1500 K and 0 kbar is also highlighted with a yellow dot. The thin dotted lines represent the 7×5 grid of crystal parameters used for free energy calculations. Experimental data is overlaid: blue triangles show room-temperature stress-pressure curve from Ref. [23], and red triangles show 0 kbar isobar data from 0 to 1300 K, as recommended in Ref. [1].

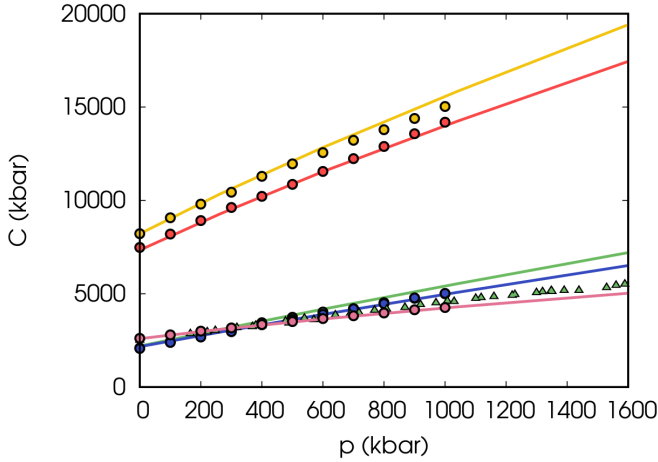


FIG. 2. Pressure-dependent ECs of osmium (PBE calculation): C_{11} (red line), C_{33} (yellow line), C_{44} (pink line), C_{12} (green line), C_{13} (blue line). Dots represent PBE calculations from Ref. [16] (same color convention). Green triangles show the experimental measurements of C_{44} from Ref. [9].

rives from phonon frequencies $\omega_\eta(\mathbf{q}, \xi)$:

$$F_{vib}(\xi, T) = \frac{1}{2N} \sum_{\mathbf{q}\eta} \hbar \omega_\eta(\mathbf{q}, \xi) + \frac{1}{N\beta} \sum_{\mathbf{q}\eta} \ln [1 - \exp(-\beta \hbar \omega_\eta(\mathbf{q}, \xi))]. \quad (2)$$

Here \hbar is the reduced Planck's constant, N is the num-

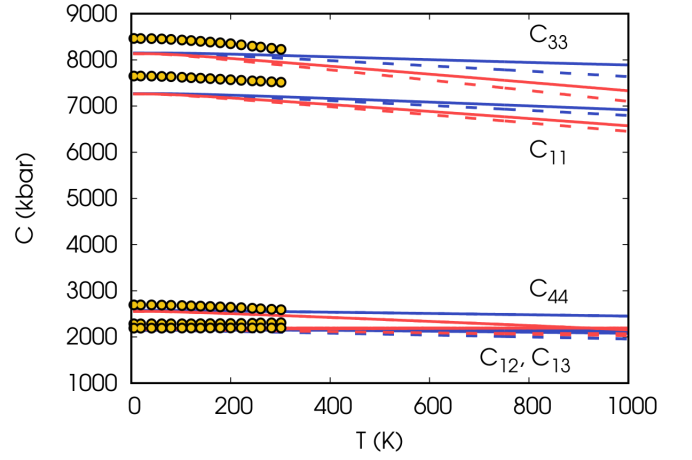


FIG. 3. TDECs of osmium (PBE calculation). Dashed lines: isothermal; solid lines: adiabatic. Blue curves: QSA; red curves: QHA. Yellow circles: experimental data from Ref. [8].

ber of cells of the solid (equal to the number of \mathbf{q} points), $\beta = \frac{1}{k_B T}$ where k_B is Boltzmann's constant, \mathbf{q} denotes phonon wavevectors, and η indexes vibrational modes. The electronic excitation term $F_{el}(\xi, T)$ follows from the density of states within the rigid-band approximation [19]. In these expressions, phonon frequencies are calculated with an electronic temperature of 0 K, and the energy $U(\xi)$ is temperature-independent. This approach assumes that electronic excitations have a minimal impact on the phonon free energy. Alternatively, electronic excitation effects can be included in $U(\xi)$ and in the phonon frequencies using Fermi-Dirac occupations at a specific temperature. However, this procedure is numerically more demanding and necessitates modifications to the free energy expression for full consistency between free energy and entropy, as discussed in Ref. [29]. In this paper, we test this procedure at 1500 K, but for all other calculations, we use phonon frequencies obtained with an electronic temperature of 0 K.

The equilibrium state under stress tensor σ emerges from minimizing the functional:

$$G_\sigma(\xi, T) = F(\xi, T) + V \sum_{j=1}^6 \sigma_j \varepsilon_j(\xi), \quad (3)$$

where V is the volume of one unit cell. We have:

$$\sigma_j = -\frac{1}{V} \frac{\partial F(\xi, T)}{\partial \varepsilon_j}. \quad (4)$$

Hence the crystal parameters that minimizes $G_\sigma(\xi, T)$ are the crystal parameters that correspond to stress σ . Using for the stress a uniform pressure p , we find the crystal parameters corresponding to each pressure at any temperature (ξ_p).

The hexagonal thermal expansion tensor contains two

independent components:

$$\alpha_{xx} = \alpha_{yy} = \frac{1}{a} \frac{da}{dT}, \quad (5)$$

$$\alpha_{zz} = \frac{1}{c} \frac{dc}{dT}, \quad (6)$$

with volume expansion $\beta = 2\alpha_{xx} + \alpha_{zz}$.

Isothermal ECs derive from second derivatives of $F(\varepsilon_i, T)$:

$$\tilde{C}_{ij}^T = \frac{1}{V} \left. \frac{\partial^2 F}{\partial \varepsilon_i \partial \varepsilon_j} \right|_T, \quad (7)$$

evaluated for five distinct strain configurations: $(\varepsilon, 0, 0, 0, 0, 0)$, $(0, 0, \varepsilon, 0, 0, 0)$, $(\varepsilon, 0, \varepsilon, 0, 0, 0)$, $(\varepsilon, \varepsilon, 0, 0, 0, 0)$, and $(0, 0, 0, \varepsilon, 0, 0)$. In these cases $\frac{1}{V} \frac{\partial^2 F}{\partial \varepsilon^2}$ gives the following combinations of ECs \tilde{C}_{11} , \tilde{C}_{33} , $\tilde{C}_{11} + \tilde{C}_{33} + 2\tilde{C}_{13}$, $2\tilde{C}_{11} + 2\tilde{C}_{12}$, and \tilde{C}_{44} respectively. When the equilibrium reference configuration has a non vanishing stress σ_{ij} , to obtain the stress-strain ECs we apply the correction [30] (in cartesian notation):

$$C_{ijkl}^T = \tilde{C}_{ijkl}^T - \frac{1}{2} \left(2\sigma_{ij}\delta_{kl} - \frac{1}{2}\sigma_{ik}\delta_{jl} - \frac{1}{2}\sigma_{il}\delta_{jk} - \frac{1}{2}\sigma_{jk}\delta_{il} - \frac{1}{2}\sigma_{jl}\delta_{ik} \right), \quad (8)$$

which simplifies for hydrostatic pressure $\sigma_{ij} = -p\delta_{ij}$ to:

$$C_{ijkl}^T = \tilde{C}_{ijkl}^T + \frac{p}{2} (2\delta_{i,j}\delta_{k,l} - \delta_{i,l}\delta_{j,k} - \delta_{i,k}\delta_{j,l}). \quad (9)$$

The second derivatives of the free energy are calculated as described in Ref. [25] taking as equilibrium configuration a subset of parameters ξ_i along the stress-pressure curve at 0 K. The values of ξ_i along this curve are given in the supplemental material, [31] together with the pressure present in each configuration. The ECs at any other set of parameters ξ_p at temperature T and pressure p are obtained by interpolation by a fourth-degree polynomial.

Adiabatic ECs follow from the transformation:

$$C_{ijkl}^S = C_{ijkl}^T + \frac{TVb_{ij}b_{kl}}{C_V}, \quad (10)$$

where b_{ij} are the thermal stresses:

$$b_{ij} = - \sum_{kl} C_{ijkl}^T \alpha_{kl}. \quad (11)$$

III. COMPUTATIONAL DETAILS

First-principles calculations are carried out within density functional theory (DFT) using the Quantum ESPRESSO package [32, 33]. Three exchange-correlation functionals are employed: the LDA, [10] the PBEsol, [34] and the PBE generalized gradient approximations. [11] While structural properties and zero-temperature ECs are computed with all three functionals, TDECs and

thermodynamic properties are evaluated exclusively with PBE.

Electron-ion interactions are treated with projector augmented wave (PAW) pseudopotentials [35] including 5s and 5p semicore states together with the 5d, 6s valence states (16 electrons per atom), with non-linear core corrections applied. [36] The pseudopotentials used are `0s.pz-spn-kjpaw_psl.1.1.0.0.UPF` (LDA), `0s.pbisol-spn-kjpaw_psl.1.1.0.0.UPF` (PBEsol) and `0s.pbe-spn-kjpaw_psl.1.1.0.0.UPF` (PBE). We expand the wavefunctions in plane waves with a cutoffs of 80 Ry (wavefunctions) and 320 Ry (charge density). The Brillouin zone integrations are made using the Methfessel-Paxton smearing ($\sigma = 0.02$ Ry) [37] with a $48 \times 48 \times 32$ \mathbf{k} -point mesh (See supplemental material [31] for a test of the convergence of elastic constants with \mathbf{k} points at 0 K). Calculations are performed on the Leonardo supercomputer at CINECA using a GPU optimized version of `thermo_pw`. [38]

The equilibrium lattice parameters are determined by minimizing the total energy on a 7×5 grid of $(a, c/a)$ values, covering pressures from -180 kbar to 2300 kbar. Phonon dispersions and Helmholtz free energies are computed in all these grid points and at seven selected points along the stress-pressure curve (Table I of the supplemental material [31]). Among these, five geometries ($i = 2, 4, 5, 6, 7$) are used to evaluate the QHA TDECs via second derivatives of the free energy with respect to strain (geometry 1 is at the highest pressure). For each geometry, five strain types are applied: base-centered orthorhombic (types 1 and 3), hexagonal (types 2 and 4) and monoclinic (type 5). Each strain is sampled at six values ($\epsilon \in [-0.0125, 0.0125]$, $\Delta\epsilon = 0.005$), requiring phonon and electronic density of states (DOS) calculations for 150 configurations.

Phonon frequencies are obtained via density functional perturbation theory (DFPT) [39, 40] on a $6 \times 6 \times 6$ \mathbf{q} -point grid, followed by Fourier interpolation onto a $200 \times 200 \times 200$ mesh for thermodynamic integration. The electronic DOS is computed on a $100 \times 100 \times 100$ \mathbf{k} -point grid.

IV. RESULTS AND DISCUSSION

We present in Tab. I the crystal parameters, the bulk modulus and the pressure derivative of the bulk modulus obtained from a Birch-Murnaghan fit of the total energy with respect to the volume along the stress-pressure curve. Assuming an experimental value of $a = 5.160$ a.u. obtained by extrapolating at 0 K the 300 K value of Ref. [23], the LDA, PBEsol and PBE errors are -0.5% , $< 0.1\%$ and 0.8% respectively, while the value of c/a is essentially accurate with all functionals. Our values are in agreement with the finding of Ref. [3] and we refer to that paper for a comparison of these values with those found in the literature.

In Tab. II we present the calculated ECs at 0 kbar and 0 K and compare the performance of the three function-

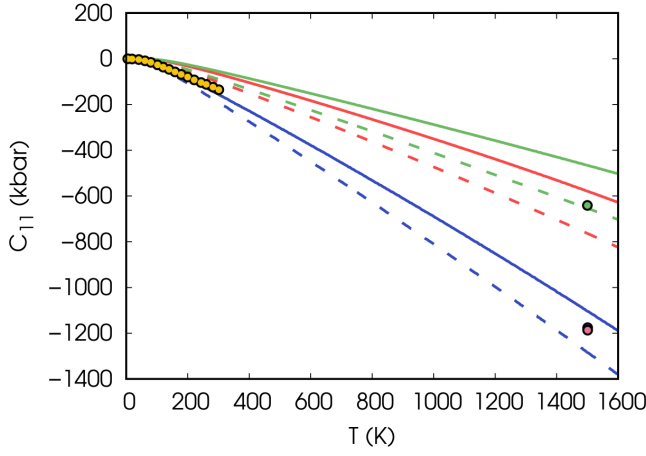


FIG. 4. Temperature dependence of the C_{11} EC of osmium (PBE calculation, with 0 K value subtracted). Dashed lines: isothermal; solid lines: adiabatic. Red (green) curves: QSA using V-ZSISA (full grid interpolation). Blue curves: QHA using V-ZSISA. Yellow circles: experimental data from Ref. [8]. Blue (green) dots at 1500 K: isothermal QHA (QSA) results at the 1500 K geometry. Pink dots at 1500 K: isothermal QHA obtained with Fermi-Dirac occupations.

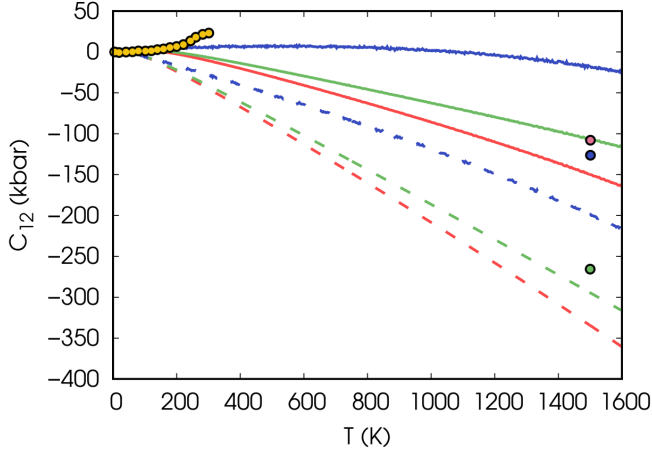


FIG. 5. Temperature dependence of the C_{12} EC of osmium (PBE calculation, with 0 K value subtracted). Line and dot conventions are identical to Fig. 4.

als with experiments and with previous calculations. In the same table we present also the bulk modulus, Young modulus, shear modulus and Poisson ratio of polycrystalline osmium obtained with the calculated ECs and the Voigt-Reuss-Hill approximation. [41] Taking the values given in Ref. [8] at 0 K as experimental values, the errors of C_{11} , C_{12} , C_{13} , C_{33} , C_{44} are 558 kbar (7%), 250 kbar (11%), 307 kbar (14%), 729 kbar (9%), and 158 kbar (6%) for LDA, they decrease to 315 kbar (4%), 134 kbar (6%), 186 kbar (9%), 475 kbar (6%), and 95 kbar (4%) for PBEsol, and further decrease to -301 kbar (-4%), -77 kbar (-3%), -10 kbar (-0.5%), -208 kbar (-2%), and -108 kbar (-4%) for PBE. We note also that zero

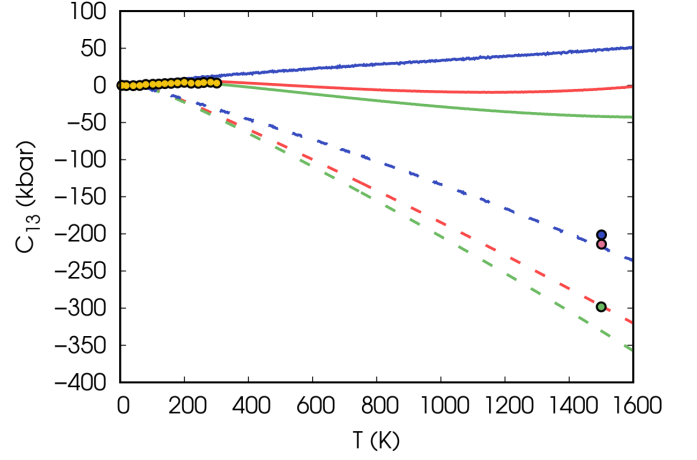


FIG. 6. Temperature dependence of the C_{13} EC of osmium (PBE calculation, with 0 K value subtracted). Line and dot conventions are identical to Fig. 4.

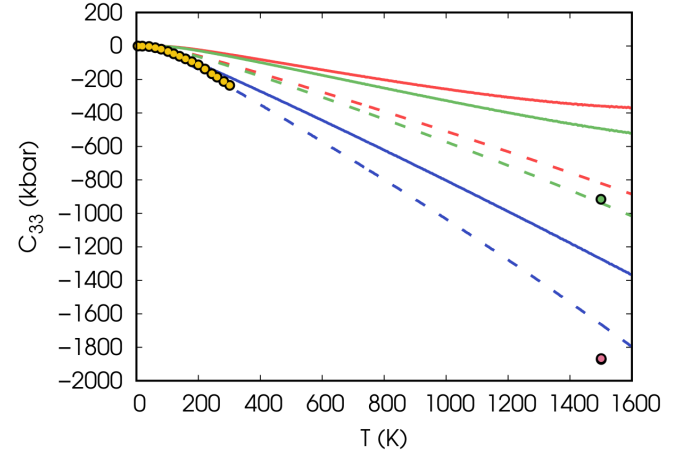


FIG. 7. Temperature dependence of the C_{33} EC of osmium (PBE calculation, with 0 K value subtracted). Line and dot conventions are identical to Fig. 4.

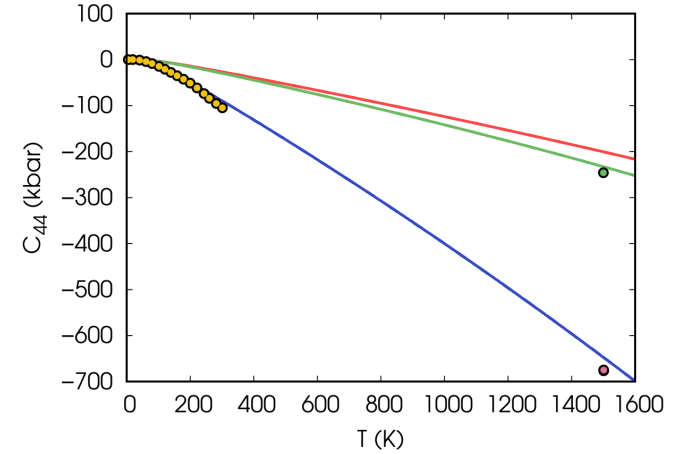


FIG. 8. Temperature dependence of the C_{44} EC of osmium (PBE calculation, with 0 K value subtracted). Line and dot conventions are identical to Fig. 4.

point motion (ZPM) decreases further the calculated ECs even for an heavy atom as osmium. We can estimate its effects from the free energy of the distorted structures in the PBE case. The decrease for C_{11} , C_{12} , C_{13} , C_{33} , and C_{44} is 70 kbar (0.9%), 14 kbar (0.6%), 8 kbar (0.4%), 89 kbar (1%), and 30 kbar (1%). When accounting for the ZPM, the PBE functional yields C_{12} , C_{13} , and C_{33} that more closely align with experimental values, while PBE and PBEsol becomes comparable for C_{11} and C_{44} . As demonstrated in our previous work, the functional selection primarily affects the ECs at 0 K, while temperature dependencies remain consistent across different functionals. Consequently, we calculated the TDECs solely using the PBE functional. Comparing the bulk moduli derived from ECs with those obtained from the equation of state, we find a reasonable agreement (the errors are 12 kbar, 11 kbar, and 8 kbar for LDA, PBEsol, and PBE, respectively).

In Fig. 1 we show the contour plots of the PBE energy, together with the stress-pressure curves at 0 K and at 1500 K. At 0 K there is a very good agreement between our data and those measured at room temperature in Ref. [23]. Note however a small shift of the pressure since with PBE the value of a at the minimum is 0.8% larger than the experiment. At variance with what found in beryllium, [17] where the 0 kbar isobar is almost parallel to the stress-pressure curve at 0 K, in osmium it is almost perpendicular. Osmium is therefore a more strict test of the V-ZSISA approximation. Moreover, both a and c/a increase with temperature while along the stress-pressure curve when a increases c/a decreases. Therefore the stress-pressure curve at 1500 K is above the 0 K one while it was below in beryllium. The predicted behavior of osmium's crystal parameters with temperature and pressure is in agreement with what found in a previous paper [3] and in experiment. [1]

In Fig. 2, we plot, at 0 K, the pressure dependent ECs in the range 0 kbar-1600 kbar and compare them with the previous theoretical PBE calculation [16] and with the recent experimental data on C_{44} [9]. There is a quite good agreement between our data and those of Ref. [16] in all the range in which they have been calculated. The agreement of C_{44} with experiment is also quite good.

We started the TDECs calculation by testing the ZSISA approximation as described in Ref. [17]. As shown in Tab. II the effect of relaxations on the ECs of osmium is quite small. Comparing the relaxed ions and the frozen ions calculations, we see that the change is $\Delta C_{11} = -\Delta C_{12} = 34$ kbar (0.4% for C_{11} and 1.5% for C_{12}). We therefore do not expect a big effect of the ZSISA approximation. We show in the supplemental material [31] that indeed the effect is quite small. Maximum differences at 1500 K are of about 10 kbar.

QSA and QHA ECs both calculated within the V-ZSISA approximation are shown in Fig. 3. C_{11} , C_{33} and C_{44} decrease more rapidly within QHA than within QSA. However, on this extended scale the experimental variation of the ECs with temperature is small and it

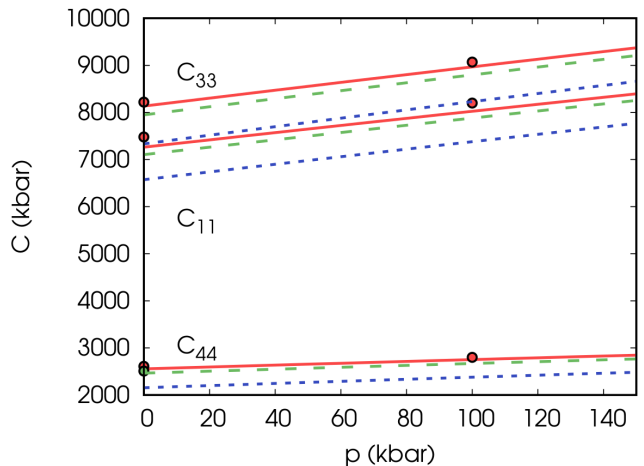


FIG. 9. PBE QHA pressure dependence of osmium adiabatic ECs C_{11} , C_{33} , and C_{44} at 4 K (red lines), 301 K (green dashed lines), 1000 K (blue dotted lines), and 1501 K (orange dot-dashed lines). Dots represent 0 K PBE calculations from Ref. [16].

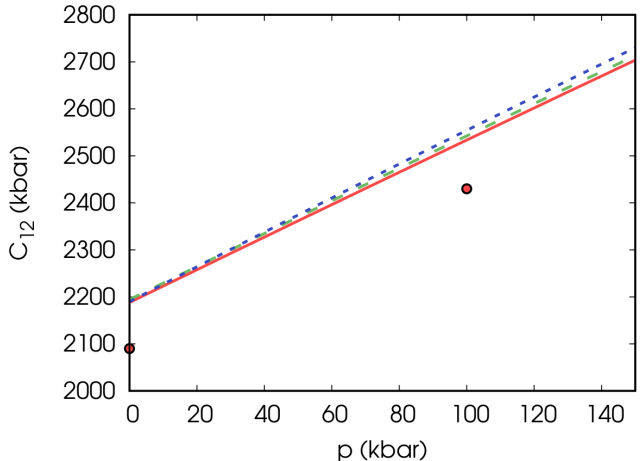


FIG. 10. PBE QHA pressure dependence of osmium adiabatic C_{12} EC. Color and line style conventions are consistent with Fig. 9.

is difficult to compare the two approximations. Both of them are in reasonable agreement with experiment. On this scale, the QSA ECs, calculated via V-ZSISA along the stress-pressure curve or beyond V-ZSISA by grid interpolation along the 0 kbar isobar, show negligible differences when the appropriate volume $V(T)$ is used for V-ZSISA interpolation at each temperature. A comparison of these approaches on this scale is included in the supplemental material, [31] while a detailed illustration is in the following figures.

The following five figures (from Fig. 4 to Fig. 8) present, in an enlarged scale, the TDECs obtained through various approximations, alongside experimental data. To facilitate comparison of temperature variation, the 0 K values have been subtracted (see the supplement-

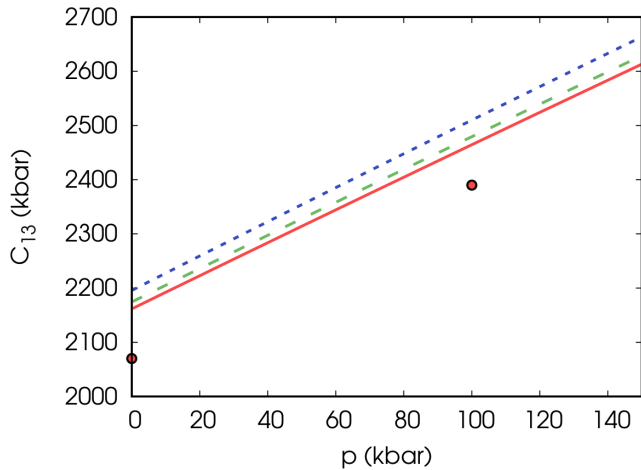


FIG. 11. PBE QHA pressure dependence of osmium adiabatic C_{13} EC. Color and line style conventions are consistent with Fig. 9.

tal material [31] for the unshifted curves). Both isothermal (dashed lines) and adiabatic (solid lines) ECs are depicted. Each figure incorporates three datasets. Firstly, the QHA ECs, derived within V-ZSISA, are represented in blue. The solid blue curve can be compared with experiments. Secondly, QSA ECs are shown. The latter are calculated within V-ZSISA, along the 0 K stress-pressure curve (red curves), and relaxing the V-ZSISA constraint, computing the ECs along the 0 kbar isobaric line (green curves). The difference between the red and green curves quantifies the effect of the V-ZSISA approximation. It is reasonable to suppose that a comparable correction should be applied to the QHA ECs, if they were computed along the 0 kbar isobar. In general the effect of V-ZSISA is not very large, although well visible on the scale of these figures.

As a singular validation test, we examined the geometry corresponding to 1500 K, as detailed in Table I. Utilizing this geometry as the equilibrium configuration, we computed the phonon frequencies for all distorted configurations and subsequently determined the second derivatives of the free energy. This methodology eliminates the need for interpolation to obtain the QHA ECs at 1500 K. The isothermal ECs derived from this approach are represented by the blue data points. Conversely, the values obtained at 4 K are the isothermal QSA at 1500 K and are indicated by green data points.

In general, across all figures, the green data point closely aligns with the isothermal QSA ECs calculated across the entire grid without the V-ZSISA approximation. The blue data point, however, exhibits a slight displacement from the V-ZSISA QHA ECs. This discrepancy is comparable to the difference observed between QSA ECs computed with V-ZSISA and those calculated across the full grid.

In the supplemental material, [31] we also quantify the effect of electronic excitations on the TDECs by compar-

ing calculations performed both with and without the electronic excitation term in the free energy. This effect proves to be quite small. We anticipate an even smaller impact when including electronic excitation effects on the phonon frequencies. As a single test, we repeated the TDEC calculation at the 1500 K geometry using Fermi-Dirac occupations at this temperature in both the DFT and phonon frequency calculations. The results are indicated by pink (QHA at 1500 K) dots in Figs. 4 to 8. As expected, the differences are minor, demonstrating that a more detailed treatment of electronic excitations is unnecessary for osmium within the investigated temperature range.

Examining each figure and comparing the ECs with experiment we can see that, with the exception of C_{12} whose increase with temperature is slightly stronger than our theoretical prediction, the temperature dependence of all the other ECs is quite well predicted by our QHA calculation. From 5 K to 301 K the experimental decrease [8] is 136 kbar (1.8%), -23 kbar (-1%), -3 kbar (-0.1 %), 236 kbar (2.8%), and 104 kbar (3.8%) for C_{11} , C_{12} , C_{13} , C_{33} , C_{44} respectively. We can compare these decreases with those predicted by QHA (within V-ZSISA) for the same ECs: 158 kbar (2.1%), -6 kbar (-0.3%), -12 kbar (-0.6%), 187 kbar (2.3%), and 90 kbar (3.5%). The QSA values (within V-ZSISA) are instead 68 kbar (0.9%), 11 kbar (0.5%), -5 kbar (-0.2%), 50 kbar (0.6%), 27 kbar (1%) more distant from the experimental data. Moreover, V-ZSISA QSA predicts a decrease of C_{12} contrary to experiment. V-ZSISA QHA predicts an increase of both C_{12} and C_{13} , in qualitative agreement with experiment.

Figs. 9, 10, and 11 illustrate the pressure dependence of the ECs at select temperatures: 4 K, 301 K, and 1000 K. We examined the pressure range from 0 kbar to 150 kbar, which is readily achievable in temperature-dependent high-pressure experiments. Within this range, the ECs exhibit a near-linear relationship with pressure at all temperatures investigated. Notably, C_{11} , C_{33} , and C_{44} decrease with increasing temperature, whereas C_{12} and C_{13} increase. The 4 K values are compared with theoretical PBE data from Ref. [16], demonstrating reasonable agreement. Differences of 112 kbar for C_{12} and 100 kbar for C_{13} are visible in Figs. 10 and 11, respectively. While a 148 kbar difference for C_{11} is present, it is not discernible within the scale of Figure 9. In contrast, the differences for C_{33} and C_{44} are considerably smaller, at 4 kbar and 25 kbar, respectively.

V. CONCLUSIONS

We have applied to osmium the computational workflow recently introduced for the calculation of the TDECs in hcp metals. [17] We presented both the QSA and the QHA results obtained using the PBE functional. Experimental data were available for comparison only within the temperature range 5 – 301 K. We observed that,

consistent with previous findings, the QHA data exhibit closer agreement with experimental results than the QSA calculations.

We evaluated the zero static internal strain approximation (ZSISA) and found it to have negligible impact on the calculated C_{11} and C_{12} ECs. Furthermore, in the QSA calculations, we examined the V-ZSISA. This approximation proved to be negligible on a large scale, but manifesting as a discernible difference on the enlarged scale employed for comparison with experimental data. Nevertheless, the QSA calculations appear to provide a reasonable quantification of the V-ZSISA effect.

The QHA results, derived via interpolation on the stress-pressure curve (within V-ZSISA), were compared with direct calculations performed at the geometry corresponding to 1500 K. Observed discrepancies were of a magnitude comparable to those encountered between the QSA V-ZSISA and full-grid interpolation. Consequently, a comprehensive full-grid interpolation of the QHA ECs for osmium, necessitating phonon calculations at 1050 distorted geometries ($7 \times 5 \times 30$), is deemed unnecessary at this moment, despite the potential for minor correc-

tions to the V-ZSISA QHA results.

Finally, we have presented the high-pressure, high-temperature ECs of osmium, with the anticipation that these data may serve as a valuable reference for future experimental measurements of these quantities.

ACKNOWLEDGMENTS

This work has been supported by the Italian MUR (Ministry of University and Research) through the National Centre for HPC, Big Data, and Quantum Computing (grant No. CN00000013). Computational facilities have been provided by SISSA through its Linux Cluster, ITCS, and the SISSA-CINECA 2021-2025 Agreement. Partial support has been received from the European Union through the MAX “Materials design at the eXascale” Centre of Excellence for Supercomputing applications (Grant agreement No. 101093374, co-funded by the European High Performance Computing joint Undertaking (JU) and participating countries 824143).

-
- [1] J. W. Arblaster, Crystallographic Properties of Osmium: Assessment of properties from absolute zero to 1300 K, *Platinum Metals Review* **57**, 177 (2013).
 - [2] C.-M. Liu, Y. Cheng, B. Zhu, and G.-F. Ji, Structural and thermodynamic properties of Os from first-principles calculations, *Physica B: Condensed Matter* **406**, 2110 (2011).
 - [3] M. Palumbo and A. Dal Corso, Lattice dynamics and thermophysical properties of h.c.p. Os and Ru from the quasi-harmonic approximation, *Journal of Physics: Condensed Matter* **29**, 395401 (2017).
 - [4] L. Burakovsky, N. Burakovsky, and D. L. Preston, Ab initio melting curve of osmium, *Physical Review B* **92**, 174105 (2015).
 - [5] A. A. Tal, M. I. Katsnelson, M. Ekholm, H. J. M. Jönsson, L. Dubrovinsky, N. Dubrovinskaia, and I. A. Abrikosov, Pressure-induced crossing of the core levels in $5d$ metals, *Physical Review B* **93**, 205150 (2016).
 - [6] L. Dubrovinsky, N. Dubrovinskaia, E. Bykova, M. Bykov, V. Prakapenka, C. Prescher, K. Glazyrin, H.-P. Liermann, M. Hanfland, M. Ekholm, Q. Feng, L. V. Pourovskii, M. I. Katsnelson, J. M. Wills, and I. A. Abrikosov, The most incompressible metal osmium at static pressures above 750 gigapascals, *Nature* **525**, 226 (2015).
 - [7] D. Koudela, M. Richter, A. Möbius, K. Koepf, and H. Eschrig, Lifshitz transitions and elastic properties of osmium under pressure, *Physical Review B* **74**, 214103 (2006).
 - [8] C. Pantea, I. Stroe, H. Ledbetter, J. B. Betts, Y. Zhao, L. L. Daemen, H. Cynn, and A. Migliori, Elastic constants of osmium between 5 and 300 K, *Physical Review B* **80**, 024112 (2009).
 - [9] Y. T. Jingyi Liu, High-pressure Raman study of osmium and rhenium up to 200 GPa and pressure dependent elastic shear modulus C44, *Chinese Physics B* **31**, 37801 (2022).
 - [10] J. P. Perdew and A. Zunger, Self-interaction correction to density-functional approximations for many-electron systems, *Physical Review B* **23**, 5048 (1981).
 - [11] J. P. Perdew, K. Burke, and M. Ernzerhof, Generalized gradient approximation made simple, *Physical Review Letters* **77**, 3865 (1996).
 - [12] L. Fast, J. M. Wills, B. Johansson, and O. Eriksson, Elastic constants of hexagonal transition metals: Theory, *Physical Review B* **51**, 17431 (1995).
 - [13] C.-Z. Fan, S.-Y. Zeng, L.-X. Li, Z.-J. Zhan, R.-P. Liu, W.-K. Wang, P. Zhang, and Y.-G. Yao, Potential superhard osmium dinitride with fluorite and pyrite structure: First-principles calculations, *Physical Review B* **74**, 125118 (2006).
 - [14] B. Minisini, J. Roetting, and F. Tsobnang, Elastic and thermodynamic properties of OsSi, OsSi₂ and Os₂Si₃, *Computational Materials Science* **43**, 812 (2008).
 - [15] R. Yu, J. Zhu, and H. Q. Ye, Calculations of single-crystal elastic constants made simple, *Computer Physics Communications* **181**, 671 (2010).
 - [16] X. H. Deng, W. Lu, Y. M. Hu, and H. S. Gu, The elastic properties of hexagonal osmium under pressure: The first-principles investigations, *Physica B: Condensed Matter* **404**, 1218 (2009).
 - [17] X. Gong and A. Dal Corso, High-temperature and high-pressure thermoelasticity of hcp metals from ab initio quasiharmonic free energy calculations: The beryllium case, *Physical Review B* **110**, 094109 (2024).
 - [18] C. Malica and A. Dal Corso, Quasi-harmonic temperature dependent elastic constants: applications to silicon, aluminum, and silver, *Journal of Physics: Condensed Matter* **32**, 315902 (2020).
 - [19] C. Malica and A. Dal Corso, Quasi-harmonic thermoe-

- lasticity of palladium, platinum, copper, and gold from first principles, *Journal of Physics: Condensed Matter* **33**, 475901 (2021).
- [20] X. Gong and A. Dal Corso, Ab initio quasi-harmonic thermoelasticity of molybdenum at high temperature and pressure, *The Journal of Chemical Physics* **160**, 244703 (2024).
- [21] X. Gong and A. Dal Corso, High-pressure and high-temperature thermoelasticity of tantalum: An ab initio study, *The Journal of Chemical Physics* **162**, 124709 (2025).
- [22] Y. Ma, T. Cui, L. Zhang, Y. Xie, G. Zou, J. S. Tse, X. Gao, and D. D. Klug, Electronic and crystal structures of osmium under high pressure, *Physical Review B* **72**, 174103 (2005).
- [23] T. Kenichi, Bulk modulus of osmium: High-pressure powder x-ray diffraction experiments under quasihydrostatic conditions, *Physical Review B* **70**, 012101 (2004).
- [24] A. Dal Corso, **thermo.pw**, can be found at the webpage <https://github.com/dalcorso/thermo.pw> (2014).
- [25] A. Dal Corso, Elastic constants of beryllium: a first-principles investigation, *Journal of Physics: Condensed Matter* **28**, 075401 (2016).
- [26] M. Palumbo and A. Dal Corso, Lattice dynamics and thermophysical properties of h.c.p. Re and Tc from the quasi-harmonic approximation, *Physica Status Solidi (B)* **254**, 1700101 (2017).
- [27] C. Malica and A. Dal Corso, Temperature-dependent atomic B factor: an ab initio calculation, *Acta Crystallographica Section A* **75**, 624 (2019).
- [28] C. Malica and A. Dal Corso, Temperature dependent elastic constants and thermodynamic properties of BAs: An ab initio investigation, *Journal of Applied Physics* **127**, 245103 (2020).
- [29] P. B. Allen, Anharmonic phonon quasiparticle theory of zero-point and thermal shifts in insulators: Heat capacity, bulk modulus, and thermal expansion, *Physical Review B* **92**, 064106 (2015).
- [30] T. H. K. Barron and M. L. Klein, Second-order elastic constants of a solid under stress, *Proceedings of the Physical Society* **85**, 523 (1965).
- [31] See Supplemental Material at URL [inserted by the publisher] that contains plots of the thermodynamic properties (thermal expansion, isobaric heat capacity, bulk modulus), several plot of temperature dependent elastic constants and a table with the crystal parameters of the 7 geometries studied along the “stress-pressure” $T = 0$ K isotherm. We display also the convergence of the elastic constants with the \mathbf{k} -points sampling.
- [32] P. Giannozzi, S. Baroni, N. Bonini, M. Calandra, R. Car, C. Cavazzoni, D. Ceresoli, G. L. Chiarotti, M. Cococcioni, I. Dabo, A. Dal Corso, S. de Gironcoli, S. Fabris, G. Fratesi, R. Gebauer, U. Gerstmann, C. Gougoussis, A. Kokalj, M. Lazzeri, L. Martin-Samos, N. Marzari, F. Mauri, R. Mazzarello, S. Paolini, A. Pasquarello, L. Paulatto, C. Sbraccia, S. Scandolo, G. Sclauzero, A. P. Seitsonen, A. Smogunov, P. Umari, and R. M. Wentzcovitch, QUANTUM ESPRESSO: a modular and open-source software project for quantum simulations of materials, *Journal of Physics: Condensed Matter* **21**, 395502 (2009).
- [33] P. Giannozzi, O. Andreussi, T. Brumme, O. Bunau, M. Buongiorno Nardelli, M. Calandra, R. Car, C. Cavazzoni, D. Ceresoli, M. Cococcioni, N. Colonna, I. Carnimeo, A. Dal Corso, S. de Gironcoli, P. Delugas, R. A. DiStasio, A. Ferretti, A. Floris, G. Fratesi, G. Fugallo, R. Gebauer, U. Gerstmann, F. Giustino, T. Gorni, J. Jia, M. Kawamura, H.-Y. Ko, A. Kokalj, E. Küçükbenli, M. Lazzeri, M. Marsili, N. Marzari, F. Mauri, N. L. Nguyen, H.-V. Nguyen, A. Otero-de-la Roza, L. Paulatto, S. Poncé, D. Rocca, R. Sabatini, B. Santra, M. Schlipf, A. P. Seitsonen, A. Smogunov, I. Timrov, T. Thonhauser, P. Umari, N. Vast, X. Wu, and S. Baroni, Advanced capabilities for materials modelling with Quantum ESPRESSO, *Journal of Physics: Condensed Matter* **29**, 465901 (2017).
- [34] J. P. Perdew, A. Ruzsinszky, G. I. Csonka, O. A. Vydrov, G. E. Scuseria, L. A. Constantin, X. Zhou, and K. Burke, Restoring the density-gradient expansion for exchange in solids and surfaces, *Physical Review Letters* **100**, 136406 (2008).
- [35] A. Dal Corso, **pslibrary**, can be found at the webpage <https://github.com/dalcorso/pslibrary> (2010).
- [36] S. G. Louie, S. Froyen, and M. L. Cohen, Nonlinear ionic pseudopotentials in spin-density-functional calculations, *Phys. Rev. B* **26**, 1738 (1982).
- [37] M. Methfessel and A. T. Paxton, High-precision sampling for brillouin-zone integration in metals, *Physical Review B* **40**, 3616 (1989).
- [38] X. Gong and A. Dal Corso, An alternative GPU acceleration for a pseudopotential plane-waves density functional theory code with applications to metallic systems, *Computer Physics Communications* **308**, 109439 (2025).
- [39] S. Baroni, S. de Gironcoli, A. Dal Corso, and P. Giannozzi, Phonons and related crystal properties from density-functional perturbation theory, *Review of Modern Physics* **73**, 515 (2001).
- [40] A. Dal Corso, Density functional perturbation theory within the projector augmented wave method, *Physical Review B* **81**, 075123 (2010).
- [41] R. E. Newnham, *Properties of Materials: Anisotropy, Symmetry, Structure* (Oxford University Press, Oxford, New York, 2004).